Three-mode resonant coupling of collective excitations in a Bose-Einstein condensate

Yong-li Ma,[1,2] Guoxiang Huang,[2,3] and Bambi Hu[2,4]

[1]*Department of Physics, Fudan University, Shanghai 200433, China*
[2]*Centre for Nonlinear Studies and Department of Physics, Hong Kong Baptist University, Hong Kong, China*
[3]*Department of Physics, East China Normal University, Shanghai 200062, China*
[4]*Department of Physics, University of Houston, Houston, Texas 77204, USA*

We make a systematic study of the resonant mode coupling of the collective excitations at zero temperature in a Bose-Einstein condensate (BEC). (i) Based on the Gross-Pitaevskii equation we derive a set of nonlinearly coupled envelope equations for a three-mode resonant interaction (TMRI) by means of a method of multiple scales. (ii) We calculate the coupling matrix elements for the TMRI and show that the divergence appearing in previous studies can be eliminated completely by using a Fetter-like variational approximation for the ground-state wave function of the condensate. (iii) We provide the selection rules in mode-mode interaction processes [including TMRI and second-harmonic generation (SHG)] according to the symmetry of the excitations. (iv) By solving the nonlinearly coupled envelope equations we obtain divergence-free nonlinear amplitudes for the TMRI and SHG processes and show that our theoretical results on the shape oscillations of the condensate agree well with the experimental ones. We suggest also an experiment to check the theoretical prediction of the present study on the TMRI of collective excitations in a BEC.

I. INTRODUCTION

Elementary excitations and their interactions are fundamental subjects in quantum many-body systems [1]. In recent years, much attention has been paid to the study of linear collective excitations in trapping and weakly interacting Bose gases [2,3] due to the remarkable experimental realization of the Bose-Einstein condensates (BECs) of cold atomic gases [4]. The interparticle interaction may result in dramatic effects and many new nonlinear excitations can appear in certain experimental conditions. The most spectacular experimental progress for the nonlinear excitations recently achieved in BECs are the observation of solitons [5,6] and vortices [7]. On the other hand, recently there is growing interest on the mode-mode resonant interactions of the excitations in trapped condensed Bose gases [8–17]. The nonlinearity, originating from the interatomic interaction, is included in the equation of motion of the order parameter through the mean field proportional to the condensate density and is expected to give various mode-coupling processes, such as second-harmonic generation (SHG), three-mode resonant interaction (TMRI), and four-wave mixing. This nonlinearity has an obvious analogy between the mode coupling in BECs and that in other contexts such in nonlinear optics.

As is well known, to develop a complete and consistent theoretical description for weakly nonlinear excitations and their interactions, a satisfactory linear theory is needed. Up to now nearly all analytical works on the linear excitations in BECs are based on the Thomas-Fermi (TF) limit by using the fact that, for large particle number and repulsive interatomic interaction, the interacting energy is dominant compared with the kinetic energy (quantum pressure) [3]. However, the use of the TF limit brings many untractable problems. (i) At the boundary of the condensate the Bogoliubov amplitude varies sharply and hence the kinetic energy of both the con-

densate and the excitations contributed from the boundary layer can not be neglected. In fact mode couplings mostly take place in the boundary layer regions [13]. (ii) A singular point appears in the solution of the Bogoliubov amplitude at the boundary of the condensate [18,19] which makes the theory uncontrollable. (iii) The existence of the singular point results in a divergence for the interacting coupling matrix elements [13,20], which are important quantities for mode-mode resonant interaction processes. (iv) A divergence occurs also in the calculation of the shape vibration of BECs. Thus a manageable, consistent theory to obtain divergence-free wave functions, coupling matrix elements, and shape vibration of the condensate for mode couplings of the excitations in trapped BECs is required. However, as far as we know, such a theory is still lacking up to now.

In a recent work we have proposed a method for finding analytical solutions of the Bogoliubov–de Gennes (BdG) equations for the low-lying collective excitations in a harmonically trapped BEC beyond the TF limit. We showed that, by using a simple variational wave function for the condensate ground state, the divergence at the boundary layer of the condensate appearing in the TF limit can be eliminated completely. We have also obtained explicit and divergence-free expressions for the eigenvalues and eigenfunctions of the linear excitations for traps with spherical and cylindrical symmetries [20]. The purpose of the present work is to present a consistent, divergence-free theoretical description for studying mode coupling of the excitations in trapped BECs. We consider mainly the energy conversion in various TMRI processes (including SHG as a particular case) for a BEC at zero temperature. In this case the Gross-Pitaevskii (GP) equation for the evolution of order parameter is a good starting point [21]. We go beyond the TF limit and provide explicit formulas for divergence-free coupling matrix elements, selection rules of the coupling matrix elements, and the solutions of the nonlinearly coupled envelope equations,

as well as the shape oscillations for describing SHG and TMRI processes with spherically and axially symmetric traps. The arrangement of the paper is as follows. We derive in Sec. II the nonlinearly coupled envelope equations for TMRI and SHG based on the time-dependent GP equation by using the method of multiple scales. In Sec. III we calculate analytically the coupling matrix elements using an eliminating divergence technique. In Sec. IV we calculate respectively the average squared widths of the shape oscillations of the condensate in the radial and the axial directions, which are divergence-free and compare well with the experimental results for SHG and TMRI processes. Section V contains a summary and discussion of our results.

II. NONLINEAR AMPLITUDE EQUATIONS FOR THE TMRIS

A. Model and asymptotic expansion

The grand canonical Hamiltonian of a weakly interacting Bose gas is given by [1–3]

$$\hat{H} = \int d^3\mathbf{r} \; \hat{\psi}^\dagger(\mathbf{r},t) \left[-\frac{\hbar^2}{2M}\nabla^2 + V_{\text{ext}}(\mathbf{r}) - \mu \right.$$
$$\left. + \frac{g}{2}\hat{\psi}^\dagger(\mathbf{r},t)\hat{\psi}(\mathbf{r},t) \right] \hat{\psi}(\mathbf{r},t), \tag{1}$$

where $\hat{\psi}(\mathbf{r},t)$ is the field operator which annihilates a boson at location $\mathbf{r}$ and time t, $g=4\pi\hbar^2 a_{\text{sc}}/M$ is the atom-atom interaction constant with M the atomic mass and a_{sc} the s-wave scattering length ($a_{\text{sc}}>0$ for a repulsive interaction), and μ is the chemical potential of the system. The anisotropic harmonic trapping potential is of the form $V_{\text{ext}}(\mathbf{r})=\frac{1}{2}M[(\omega_x^2 x^2+\omega_y^2 y^2+\omega_z^2 z^2)]$, where ω_j $(j=x,y,z)$ is the frequency of the trap in the jth direction. The Heisenberg equation of motion for $\hat{\psi}$ reads

$$i\hbar\frac{\partial\hat{\psi}}{\partial t} = \left[-\frac{\hbar^2}{2M}\nabla^2 + V_{\text{ext}}(\mathbf{r}) - \mu + g\psi^\dagger\hat{\psi} \right]\hat{\psi} \tag{2}$$

with the commutation relation $[\hat{\psi}(\mathbf{r},t),\hat{\psi}^\dagger(\mathbf{r}',t)]=\delta(\mathbf{r}-\mathbf{r}')$ and other commutators zero. At low temperature the dynamics of a Bose-condensed gas is well described by the time-dependent GP equation, which can be obtained from Eq. (2) by taking $\hat{\psi}(\mathbf{r},t)=\psi(\mathbf{r},t)+\hat{\psi}'(\mathbf{r},t)$, where $\psi(\mathbf{r},t)$ and $\hat{\psi}'(\mathbf{r},t)$ describe, respectively, the condensed and thermal components and their fluctuations. For a dilute gas at zero temperature one can neglect the thermal component and its fluctuations. Thus we have

$$i\hbar\frac{\partial\psi}{\partial t} = \left[-\frac{\hbar^2}{2M}\nabla^2 + V_{\text{ext}}(\mathbf{r}) - \mu + g|\psi|^2 \right]\psi. \tag{3}$$

To find the excitations from a static condensate we take

$$\psi(\mathbf{r},t) = \psi_G(\mathbf{r}) + \varepsilon\phi(\mathbf{r},t), \tag{4}$$

where $\psi_G(\mathbf{r})$ is the ground-state wave function, $\phi(\mathbf{r},t)$ describes the excitations generated from the condensate, and ε is a parameter denoting the relative amplitude of the excitations. Then Eq. (3) becomes

$$i\hbar\frac{\partial\phi}{\partial t} = (\hat{H}_0 - \mu)\phi + g[\psi_G^2(2\phi + \phi^*)$$
$$+ \varepsilon\psi_G(\phi^2 + 2\phi^*\phi) + \varepsilon^2\phi^*\phi^2], \tag{5}$$

where $\hat{H}_0 = -\hbar^2\nabla^2/(2M) + V_{\text{ext}}(\mathbf{r})$ and ψ_G satisfies the equation

$$(\hat{H}_0 - \mu + g\psi_G^2)\psi_G = 0. \tag{6}$$

We consider weak nonlinear excitations from a BEC; thus ε is a small parameter characterizing the amplitude of the excitations. To derive nonlinear amplitude equations we use the method of multiple scales [22]. Let $\phi=\phi^{(1)}+\varepsilon\phi^{(2)}+\cdots$ with $\phi^{(j)}=\phi^{(j)}(\mathbf{r},t,\tau)$, where $\tau=\varepsilon t$. Then Eq. (5) becomes

$$\hat{O}\phi^{(j)} \equiv i\hbar\frac{\partial\phi^{(j)}}{\partial t} - (\hat{H}_0 - \mu)\phi^{(j)} - g\psi_G^2(2\phi^{(j)} + \phi^{(j)*}) = Q^{(j)}, \tag{7}$$

with $Q^{(1)}=0$ and $Q^{(2)}=-i\hbar\partial\phi^{(1)}/\partial\tau - g\psi_G^2(2\phi^{(1)}+\phi^{(1)*})$. The higher-order $Q^{(j)}$ $(j=3,4,\ldots)$ are not needed and thus are omitted here.

B. Nonlinear amplitude equations for the TMRI

At the leading order $(j=1)$ Eq. (7) reads $\hat{O}\phi^{(1)}=0$. To solve this (variable-coefficient) equation we make the following Bogoliubov decomposition:

$$\phi^{(1)}(\mathbf{r},t) = \sum_{n=0}^{\infty} [u_n(\mathbf{r})b_n(\tau)\exp(-i\omega_n t) + v_n^*(\mathbf{r})b_n^*(\tau)\exp(i\omega_n t)], \tag{8}$$

where b_n is the amplitude depending on the slowly varying time τ, and $u_n(\mathbf{r})$ and $v_n(\mathbf{r})$ are obtained by sovling the BdG eigenvalue equations

$$\hat{L}u_n(\mathbf{r}) + g\psi_G^2 v_n(\mathbf{r}) = + E_n u_n(\mathbf{r}), \tag{9}$$

$$\hat{L}v_n(\mathbf{r}) + g\psi_G^2 u_n(\mathbf{r}) = - E_n v_n(\mathbf{r}), \tag{10}$$

where $E_n=\hbar\omega_n$ is the eigenvalue and the operator $\hat{L}$ is defined by $\hat{L}=\hat{H}_0-\mu+2g\psi_G^2$. From the BdG equations (9) and (10) it is easy to show the eigenfunctions $u_n(\mathbf{r})$ and $v_n(\mathbf{r})$ satisfy the following orthogonality relations:

$$\int d^3\mathbf{r}[u_n^*(\mathbf{r})u_{n'}(\mathbf{r}) - v_n^*(\mathbf{r})v_{n'}(\mathbf{r})] = \delta_{nn'}, \tag{11}$$

$$\int d^3\mathbf{r}[u_n(\mathbf{r})v_{n'}(\mathbf{r}) - u_{n'}(\mathbf{r})v_n(\mathbf{r})] = 0. \tag{12}$$

By choosing the zero modes (i.e., the modes with zero eigenvalues) suitably one can obtain a complete set of eigenfunctions, which is the key for diagonalizing a Bogoliubov (quadratic) Hamiltonian and studying the interaction of the collective excitations in the high-order approximation [20]. Here we are interested in a TMRI of excitations in the BEC

and thus the first-order approximated solution should be chosen as

$$\phi^{(1)} = \sum_{n=1}^{3} [u_n(\mathbf{r})b_n(\tau)\exp(-i\omega_n t) + v_n^*(\mathbf{r})b_n^*(\tau)\exp(i\omega_n t)],$$
(13)

where ω_1, ω_2, and ω_3 are selected to satisfy the three-mode resonant condition $\omega_3 = \omega_2 + \omega_1 + \tilde{\Delta}_3$ with $\tilde{\Delta}_3 = \varepsilon\Delta_3$ a possible frequency mismatch in the TMRI process.

At the second order ($j=2$) the solvability conditions of the equation $\hat{O}\phi^{(2)} = Q^{(2)}$ yield the nonlinearly coupled envelope equations controlling the evolution of b_n ($n=1,2,3$):

$$i\hbar\frac{db_1}{d\tau} = (A_{132} + B_{123})b_2b_3\exp(-i\Delta_3\tau),$$
(14)

$$i\hbar\frac{db_2}{d\tau} = (A_{231} + B_{213})b_3b_1\exp(-i\Delta_3\tau),$$
(15)

$$i\hbar\frac{db_3}{d\tau} = (D_{312} + D_{321})b_1b_2\exp(i\Delta_3\tau),$$
(16)

where the coefficients are given by

$$A_{nn_1n_2} = gN_0 \int d^3\mathbf{r}\, \psi_G[u_n^*(u_{n_1} + v_{n_1})v_{n_2}^* + v_{n_1}(v_{n_2}^* + u_{n_2}^*)v_n^*$$
$$+ v_{n_1}(v_n^* + u_n^*)v_{n_2}^*],$$
(17)

$$B_{nn_1n_2} = gN_0 \int d^3\mathbf{r}\, \psi_G[u_{n_1}^*(u_{n_2} + v_{n_2})v_n^* + u_{n_1}^*(v_n^* + u_n^*)u_{n_2}$$
$$+ u_n^*(v_{n_1}^* + u_{n_1}^*)u_{n_2}],$$
(18)

$$C_{nn_1n_2} = gN_0 \int d^3\mathbf{r}\, \psi_G[u_n^*(v_{n_1}^* + u_{n_1}^*)v_{n_2}^* + u_{n_1}^*(v_n^* + u_n^*)v_{n_2}^*$$
$$+ u_{n_1}^*(v_{n_2}^* + u_{n_2}^*)v_n^*],$$
(19)

$$D_{nn_1n_2} = gN_0 \int d^3\mathbf{r}\, \psi_G[u_n^*(u_{n_1} + v_{n_1})u_{n_2} + v_{n_1}(u_{n_2} + v_{n_2})v_n^*$$
$$+ v_{n_1}(v_n^* + u_n^*)u_{n_2}].$$
(20)

It is easy to show that one has the relation $A_{132} + B_{123} = A_{231} + B_{213} = 2(D_{312} + D_{321})^* = gN_0M_3$, where the coupling matrix element M_3 for the TMRI process is given by

$$M_3 = \int d^3\mathbf{r}\, \psi_G[u_3^*(u_1 + v_1)u_2 + v_1(u_2 + v_2)v_3^*$$
$$+ v_2(v_3^* + u_3^*)u_1].$$
(21)

As a special case, the envelope equations for a SHG read

$$i\hbar\frac{db_1}{d\tau} = (A_{121} + B_{112})b_1b_2\exp(-i\Delta_2\tau),$$
(22)

$$i\hbar\frac{db_2}{d\tau} = D_{211}b_1b_1\exp(i\Delta_2\tau),$$
(23)

where $\varepsilon\Delta_2 = \omega_2 - 2\omega_1$ is a frequency mismatch. The coefficients in Eqs. (22) and (23) satisfy $A_{121} + B_{112} = 2D_{211}^* = gN_0M_2$ with

$$M_2 = \int d^3\mathbf{r}\, \psi_G[u_2^*(u_1 + v_1)u_1 + v_1(u_1 + v_1)v_2^*$$
$$+ v_1(v_2^* + u_2^*)u_1],$$
(24)

which is the coupling matrix element for the SHG process [23,24].

III. CALCULATION OF THE COUPLING MATRIX ELEMENTS FOR SPHERICALLY AND AXIALLY HARMONIC TRAPS

A. Solutions of the BdG equations

In order to investigate the TMRI and SHG of the collective excitations, we must make a detailed calculation of the important physical quantities, i.e., the coupling matrix elements M_3 and M_2. This requires solving BdG equations (9) and (10) to get the related eigenfunctions. Previous studies [13] show that one cannot avoid a divergence when calculating the coupling matrix elements if using the the BdG eigenfunctions obtained under the TF limit [18]. Here we employ results obtained beyond the TF limit [20] [i.e., the TF regime; we designate the TF regime as $P \gg 1$ and the TF limit as $P \to \infty$, where $P \equiv N_0 a_{sc}/a_{HO}$ is the atom-atom interaction strength, N_0 is the particle number in the condensate, and $a_{HO} \equiv (\hbar/M\omega_\perp)^{1/2}$ is the characteristic oscillator length of the trapping potential] to study the TMRI and the SHG of the excitations in a BEC with a harmonic trap. In that work we obtained all possible eigensolutions of Eqs. (9) and (10) in spherically and axially symmetric harmonic potentials by using an exactly solvable model in the TF regime. The key for getting these divergence-free results is the use of a properly chosen trial wave function for the condensate ground state, thereby avoiding the appearance of a singularity at the boundary layer of the condensate as is often encountered in the TF limit. In the following we give a simple description of some results related to the ground-state wave function and the eigenfunctions of the BdG equations obtained in Ref. [20].

For an axially symmetric trap, we define $\bar{r}^2 = \bar{s}^2 + \lambda^2\bar{z}^2$ ($\lambda = 1$ is only a special case for a spherical trap); a Fetter-like trial wave function $\psi_G = C_G\sqrt{\lambda}(1-\bar{r}^2)^{(q+1)/2}\Theta(1-\bar{r})$ is carefully chosen, where $C_G = [\lambda N_0/2\pi R_\perp^3 B(3/2, 2+q)]^{1/2}$ is a normalization constant and $B(p,q)$ is the beta function [25]. The ratio $R_\perp/a_{HO}$ and the chemical potential take the simple forms $R_\perp/a_{HO} = [4\lambda P/B(3/2, 2+q)]^{1/5}$ and $\mu \simeq \frac{1}{2}\hbar\omega_\perp[4\lambda P/B(3/2, 2+q)]^{2/5}$ in the TF regime. The variation parameter q is selected by minimizing the ground-state energy and hence satisfies a constraint condition, i.e., $(2+\lambda^2)(AR_\perp^{-2})' + 3(BR_\perp^2)' + 4\lambda^2 P(CR_\perp^{-3})' = 0$, where A, B, and C are functions of q and the prime denotes the derivative with respect to q [20].

By introducing the parameter $\zeta = \hbar\omega_\perp/2\mu \ll 1$, the BdG equations (9) and (10) are solved analytically by defining the new functions $\varphi_\pm(\mathbf{r}) \equiv u(\mathbf{r}) \pm v(\mathbf{r})$. For $\lambda = 1$ (i.e., spherical trap), good quantum numbers are the principal quantum number n_r $(=0,1,2,\ldots)$, the angular quantum number l $(=0,1,2,\ldots)$, and the magnetic quantum number m $(=0,\pm 1, \pm 2, \ldots, \pm l)$. Since the excitation spectra are independent of m, the entire excitation modes are labeled by two quantum numbers n_r and l, called the $(n_r l)$ modes. The normalized solutions of the BdG equations under the normalization condition $\int d^3\mathbf{r}(u_n^2 - v_n^2) = 1$ are [20]

$$\varphi_\pm(\mathbf{r}) = [2/(I_{n_r l} R_\perp^3)]^{1/2} (\zeta \bar{\omega}_{n_r l}^{(0)})^{\pm 1/2} (1 - \bar{r}^2)^{(q \mp 1)/2} W(\mathbf{r}),$$
(25)

with $W(\mathbf{r}) \equiv \bar{r}^l P_{n_r l}(\bar{r}^2) Y_{lm}(\theta, \varphi)$, where $Y_{lm}(\theta, \varphi)$ are spherical harmonic functions. $P_{n_r l}$ are special hypergeometric series or classical n_r th-order Jacobi polynomials defined by

$$P_{n_r l}(x) = F(-n_r, n_r + l + q + 1/2, \bar{r}^2)$$
$$= n_r B[n_r, l + 3/2] P_{n_r}^{(l+1/2, q)}(1 - 2x),$$

which form a complete set of orthonormal functions in the interval $0 \leqslant x \leqslant 1$ with weight $x^{l+1/2}(1-x)^q$. The normalization integral in the radial direction is

$$I_{n_r l} \equiv \int_0^1 dx \, x^{l+1/2}(1-x)^q P_{n_r l}^2(x)$$
$$= (l+1/2)^2/(2n_r + l + q + 3/2) B\left(n_r + 1, l + \tfrac{1}{2}\right)$$
$$\times B\left(n_r + 1 + q, l + \tfrac{1}{2}\right).$$

The eigenfrequencies $\bar{\omega}_{n_r l}$ including the first-order correction have been given explicitly in Eq. (10) of Ref. [20]. In the leading order one has $(\bar{\omega}_{n_r l}^{(0)})^2 = (\bar{\omega}_{n_r l}^{\mathrm{TF}})^2 + (2n_r + l)q$ with $(\bar{\omega}_{n_r l}^{\mathrm{TF}})^2 = 2n_r^2 + 2n_r l + 3n_r + l$ (the result in the TF limit). Here we have defined $\bar{\omega}_n \equiv \omega_n/\omega_\perp$.

For $\lambda \neq 1$ (axially harmonic trap), a good principal quantum number n_p $(=0,1,2,\ldots$ still exists) [26]. Let m be an azimuthal quantum number $(m = 0, \pm 1, \pm 2, \ldots)$, n_s the radial quantum number $(n_s = 0, 1, 2, \ldots, \mathrm{int}[n_p/2])$, and n_z the axial quantum number $(n_z = n_p - 2n_s)$. The entire excitation modes can be labeled by three quantum numbers n_z, n_s, and m, called the $(n_z n_s m)$ modes. The normalized eigenfunctions are given by

$$\varphi_\pm(\mathbf{r}) = \frac{(\zeta \bar{\omega}_{n_z n_s m}^{(0)})^{\pm 1/2}}{\sqrt{2\pi R_\perp^3 I_{n_z n_s m}}} (1 - \bar{s}^2 - \lambda^2 \bar{z}^2)^{(q \mp 1)/2} W(\mathbf{r}) \quad (26)$$

with function $W(\mathbf{r}) \equiv \bar{s}^m P_{n_p}^{(2n_s)}(\bar{s}, \bar{z}) e^{im\varphi}$. The polynomials $P_{n_p}^{(2n_s)}(\bar{z}, \bar{s}) = \sum_{k=0}^{n_p} \sum_{n=0}^{\mathrm{int}[k/2]} b_{k,n} \bar{z}^{k-2n} \bar{s}^{2n}$ form an orthonormal function set in the interval $0 \leqslant \bar{r} \leqslant 1$ with the weight $\bar{s}^m (1 - \bar{r}^2)^q$. The squares of the zero-order eigenvalues $(\bar{\omega}_{n_z n_s m}^{(0)})^2$ are the solutions of a standard continued fraction equation [20,26]. The normalization integral reads $I_{n_z n_s m} \equiv 2\int_0^1 \bar{s} \, d\bar{s} \int_0^{\sqrt{1-\bar{s}^2}/\lambda} d\bar{z} \, \bar{s}^{2m} (1 - \bar{s}^2 - \lambda^2 \bar{z}^2)^q [P_{n_p}^{(2n_s)}(\bar{z}, \bar{s})]^2$. The ei-

genvalues including the first-order correction are expressed explicitly in Eq. 16 in Ref. [20].

B. Expressions for the coupling matrix elements

Since the characteristic time scale for the energy transfer among different exciting modes is inversely proportional to the absolute value of the matrix element, we define the dimensionless coupling matrix elements $\bar{M}_k = M_k a_{\mathrm{HO}}^3$ ($k = 2, 3$). This definition of $\bar{M}_k$ differs both from [13] and from [27] since the dependence of M_k on the atom-atom interaction strength P and trap anisotropy λ is also contained in the quantity $R_\perp^{-3} \zeta^{-1/2}$. Therefore we look for the dependence of $\bar{M}_k$ on P and λ by introducing an independent volume a_{HO}^3.

We first recapitulate the case of a spherically symmetric trap (i.e., $\lambda = 1$). According to the solution (25), the coupling matrix element (21) for the TMRI reads

$$\bar{M}_3 = \frac{[4P/B(3/2, 2+q)]^{1/10}}{4\pi \sqrt{I_1 I_2 I_3 \bar{\omega}_1 \bar{\omega}_2 \bar{\omega}_3}}$$
$$\times \sqrt{\frac{N_0}{P}} \int d^3\mathbf{r} (1-\bar{r}^2)^{2q} W_1 W_2 W_3^*$$
$$\times \left[3\zeta^2 \frac{\bar{\omega}_1 \bar{\omega}_2 \bar{\omega}_3}{1-\bar{r}^2} - \bar{\Delta}_3 (1-\bar{r}^2) \right]. \quad (27)$$

The coupling matrix element (24) for the SHG is given by

$$\bar{M}_2 = \frac{[4P/B(3/2, 2+q)]^{1/10}}{4\pi I_1 \bar{\omega}_1 \sqrt{I_2 \bar{\omega}_2}}$$
$$\times \sqrt{\frac{N_0}{P}} \int d^3\mathbf{r} (1-\bar{r}^2)^{2q} W_1^2 W_2^*$$
$$\times \left[3\zeta^2 \frac{\bar{\omega}_1^2 \bar{\omega}_2}{1-\bar{r}^2} - \bar{\Delta}_2 (1-\bar{r}^2) \right]. \quad (28)$$

In Eqs. (27) and (28), $I_n = I_{n_r l}$ for $n = 1, 2, 3$ and the integral range is in the sphere $0 \leqslant \bar{r} \leqslant 1$. We note that the term proportional to ζ^2 make the integrals (27) and (28) divergent in the TF limit (i.e., $q = 0$). However, in the TF regime (i.e., $q \ll 1$), the factor $(1-x)^{2q}$ makes the integrals finite. We also note that in the case on resonance ($\bar{\Delta}_k = 0, k = 2, 3$), the only contribution to $\bar{M}_k$ comes from this term, although the value is small due to $\zeta^2 \ll 1$. In such a case the coupling is strongest at the boundary of the condensate due to the radial integrand factor $(1-\bar{r}^2)^{2q-1}$.

For the case of an axially symmetric trap (i.e., $\lambda \neq 1$), we define $x = \bar{s}^2$ and $y = \lambda \bar{z}/\sqrt{1-x}$. Then by using Eq. (26) we obtain the divergence-free coupling matrix elements for the TMRI as

$$\bar{M}_3 = \frac{[4P/B(3/2, 2+q)]^{1/10}}{16\pi^2 \lambda^{9/10} \sqrt{I_1 I_2 I_3 \bar{\omega}_1 \bar{\omega}_2 \bar{\omega}_3}}$$
$$\times \sqrt{\frac{N_0}{P}} \int_0^1 dx \int_0^1 dy \int_0^{2\pi} d\varphi \, W_1 W_2 W_3^*$$
$$\times [3\zeta^2 \bar{\omega}_1 \bar{\omega}_2 \bar{\omega}_3 (1-x)^{2q-1/2} (1-y^2)^{2q-1}$$

$$- \bar{\Delta}_3 (1-x)^{2q+3/2}(1-y^2)^{2q+1}], \tag{29}$$

the coupled matrix elements for the SHG as

$$\bar{M}_2 = \frac{[4P/B(3/2,2+q)]^{1/10}}{16\pi^2 \lambda^{9/10} I_1 \bar{\omega}_1 \sqrt{I_2 \bar{\omega}_2}} \sqrt{\frac{N_0}{P}} \int_0^1 dx \int_0^1 dy \int_0^{2\pi} d\varphi \, W_1^2 W_2^*$$

$$\times [3\zeta^2 \bar{\omega}_1^2 \bar{\omega}_2 (1-x)^{2q-1/2}(1-y^2)^{2q-1}$$

$$- \bar{\Delta}_2 (1-x)^{2q+3/2}(1-y^2)^{2q+1}] \tag{30}$$

with $I_n = I_{n_\zeta n_s m}$ for $n = 1, 2, 3$.

C. Selection rules for the coupling matrix elements

To get an efficient energy transfer among different modes in the TMRI and SHG processes, on the one hand the frequency-matching (phase-matching) conditions $\omega_3 = \omega_2 + \omega_1$ (for the TMRI) and $\omega_2 = 2\omega_1$ (for the SHG) should be satisfied. On the other hand we note that, in order to have an effective mode mixing, the coupling matrix elements must be nonzero, which imposes also another requirement of an overlap among the corresponding spatial wave functions, i.e., the symmetry arguments of the excited states select the certain modes at or close to the resonant conditions, which makes $M_2 \neq 0$ for the SHG and $M_3 \neq 0$ for the TMRI.

For the axial symmetry trap ($\lambda \notin 1$), nonzero azimuthal angular integrals for some quantum numbers m_n select a certain transition and give a set of corresponding m_n for the nth modes ($n = 1, 2, 3$). For the SHG, because $\bar{M}_2 \propto \int_0^{2\pi} e^{i(2m_1 - m_2)\varphi} d\varphi$, a nonzero $\bar{M}_2$ results in the selection rule for the quantum number

$$m_2 = 2m_1. \tag{31}$$

Similarly, for the TMRI because $\bar{M}_3 \propto \int_0^{2\pi} e^{i(m_1 + m_2 - m_3)\varphi} d\varphi$, a nonzero $\bar{M}_3$ requires

$$m_3 = m_2 + m_1. \tag{32}$$

In the case of the spherical symmetry trap ($\lambda = 1$), since the excitation spectra are independent of m, we can take $m = 0$ in Eqs. (27) and (28). Selection on the angular quantum numbers l_k is from the integral in the θ direction. For the SHG, $\bar{M}_2 \propto \int_0^\pi W_1^2 W_2^* \sin\theta d\theta \propto \int_{-1}^{+1} P_{l_1}^2(x) P_{l_2}(x) dx$ ($x = \cos\theta$). Thus the selection rule is

$$l_2 = 2l (l = 0, 1, 2, \ldots, l_1), \tag{33}$$

where l_1 and l_2 are the angular quantum numbers for the lower- and higher-lying modes, respectively. In obtaining this selection rule, we have used one property of the Legendre polynomial $P_l(x)$ so that the integration $\int_{-1}^{+1} x^k P_l(x) dx$ has a nonzero value for $k = l + 2j$ and vanishes for $k < l$ or $k = l + 2j + 1$, where $j = 0, 1, 2, \ldots$. For the TMRI, without loss of generality we take the order of $0 \le l_1 \le l_2 \le l_3$ for the given three modes, where modes $(n_{r_k} l_k)$ satisfy the frequency-matching condition. Since $\bar{M}_3 \propto \int_0^\pi W_1 W_2 W_3^* \sin\theta d\theta \propto \int_{-1}^{+1} P_{l_1}(x) P_{l_2}(x) P_{l_3}(x) dx$, by using the property of the Legendre polynomial we have the general selection rule

$$l_3 = l_1 + l_2 - 2l \quad (l = 0, 1, 2, \ldots, l_0, 2l_0 \le l_1). \tag{34}$$

Obviously, we have nonzero matrix elements in the following particular cases: (i) $l_3 = 0$ if $l_1 = l_2 = 0$; (ii) $l_3 = l_2$ if $l_1 = 0$; (iii) $l_3 = l_1 + l_2$; (iv) $l_1 = l_2 = l_3 = 2l$ for $l = 0, 1, 2, \ldots$; and (v) $l_3 = 2(l_1 - l)$ for $l = 0, 1, 2, \ldots, \text{int}[l_1/2]$ if $l_1 = l_2 > 0$.

D. Calculation of the coupling matrix elements

For the given modes close to the frequency-matching conditions and satisfying the selection rules presented above, one can make a calculation for the (dimensionless) coupling matrix elements based on Eqs. (27)–(30). The concrete expressions for the radial and axial integrands of the matrix elements can be obtained easily. In this subsection we take some examples to provide the dimensionless matrix elements for the TMRI and the SHG after carrying out the radial and axial integrals explicitly.

For the spherically symmetric trap ($\lambda = 1$), we first choose three $n_r l$ modes 10, 05, and 15 for the TMRI. Their functions are $W_1 = [1 - (5 + 2q)/3\bar{r}^2] Y_{00}$, $W_2 = \bar{r}^5 Y_{50}$ and $W_3 = [1 - (15 + 2q)/13\bar{r}^2]\bar{r}^5 Y_{50}$. The corresponding normalization integrals are given by $I_1 = [2(5+2q)/3(7+2q)]B(\frac{3}{2}, 2+q)$, $I_2 = B(\frac{13}{2}, 1+q)$, and $I_3 = [2(15+2q)/13(17+2q)]B(\frac{13}{2}, 2+q)$. The explicit expression for the dimensionless coupling matrix elements then becomes

$$\bar{M}_3 = \frac{[4P/B(3/2, 2+q)]^{1/10}}{8\pi\sqrt{I_1 I_2 I_3 \bar{\omega}_1 \bar{\omega}_2 \bar{\omega}_3}} \sqrt{\frac{N_0}{P}}$$

$$\times \left\{ 3\zeta^2 \bar{\omega}_1 \bar{\omega}_2 \bar{\omega}_3 \left[B\left(\frac{13}{2}, 2q\right) - \frac{2}{39}(55 + 16q)B\left(\frac{15}{2}, 2q\right) \right.\right.$$

$$\left. + \frac{1}{39}(75 + 40q + 4q^2)B\left(\frac{17}{2}, 2q\right) \right] - \bar{\Delta}_3 \left[B\left(\frac{13}{2}, 2+2q\right) \right.$$

$$- \frac{2}{39}(55 + 16q)B\left(\frac{15}{2}, 2+2q\right) + \frac{1}{39}(75 + 40q + 4q^2)$$

$$\left.\left. \times B\left(\frac{17}{2}, 2+2q\right) \right] \right\}. \tag{35}$$

Substituting the expressions for ζ, $\bar{\omega}_k$ ($k = 1, 2, 3$), and the function $q(P)$ into Eq. (35), we obtain the theoretical curve $\bar{M}_3(P)$, plotted in Fig. 1, by taking $N_0 = 10^6$. Note that due to the weight factor $(1-x)^{2q}$ the divergence in the integral (27) is eliminated completely. This point can also be seen clearly from the ζ^2 term in Eq. (35) for the resonant case ($\bar{\Delta}_3 = 0$): $\bar{M}_3 \propto \zeta^2/q$ and $\zeta^2/q \propto P^{-2/5} \to 0$ in the TF limit (i.e., $P \to \infty$ or $q \to 0$). Although $B(p, q)$ has a singularity as $1/q$ at $q = 0$, the result for the matrix elements is divergence-free. Figure 1 shows that $\bar{M}_3(P)$ is a decreasing function with increasing atom-atom interaction strength P. $\bar{M}_3(P) > 0$ means a negative initial population amplitude. The numerical results show that the term proportional to ζ^2 in Eq. (35) dominates the TMRI process even far from resonance or at large enough P closing on the TF limit, where the contribution from the term proportional to $\bar{\Delta}_3$ still remains small.
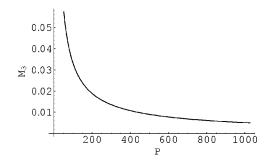
FIG. 1. The TWRI dimensionless coupling matrix element $\bar{M}_3(P)$ as a function of P (atom-atom interaction strength) for N_0 (particle number in the condensate) of 10^6 with a spherical symmetry trap. The three $n_r l$ modes are 10, 05, and 15, respectively.

We next choose two $n_r l$ modes 01 and 10 for the SHG. Their functions are $W_1 = \bar{r}Y_{10}$ and $W_2 = [1 - (5+2q)/3\bar{r}^2]Y_{00}$. The corresponding normalization integrals are given by $I_1 = B\left(\frac{5}{2}, 1+q\right)$ and $I_2 = [2(5+2q)/3(7+2q)]B\left(\frac{3}{2}, 2+q\right)$. We get

$$\bar{M}_2 = \frac{[4P/B(3/2, 2+q)]^{1/10}}{8\pi I_1 \bar{\omega}_1 \sqrt{I_2 \bar{\omega}_2}} \sqrt{\frac{N_0}{P}} \left\{ \zeta^2 \bar{\omega}_1^2 \bar{\omega}_2 \left[3B\left(\frac{5}{2}, 2q\right) \right. \right.$$
$$\left. - (5+2q)B\left(\frac{7}{2}, 2q\right) \right] - \bar{\Delta}_2 \left[B\left(\frac{5}{2}, 2+2q\right) \right.$$
$$\left. \left. - \frac{5+2q}{3}B\left(\frac{7}{2}, 2+2q\right) \right] \right\}. \tag{36}$$

Figure 2 shows the $\bar{M}_2(P)$ curve with $N_0 = 10^6$. It is shown that the ζ^2 term in Eq. (36) dominates the SHG process. There is a resonant nonlinear coupling between the lower-lying (01) and higher-lying (10) modes. The resonance is determined by $2\omega_1 = \omega_2$ and it is most efficient for $P < 400$.

For the case of axial symmetry ($\lambda \ne 1$), we take $N_0 = 10^6$ and $P = 100$ (which means taking $a_{HO}/a_{sc} = 10^4$ for most experiments) and study the geometric effect of the trap on the dimensionless coupling matrix elements. We first choose three $n_z n_s m$ modes 001, 002, and 103 in the TMRI. Their excitation spectra at leading-order approximation are $\bar{\omega}_1^{(0)} = \sqrt{1+q}$, $\bar{\omega}_2^{(0)} = \sqrt{2+2q}$, and $\bar{\omega}_3^{(0)} = \sqrt{(3+\lambda^2)(1+q)}$. The functions are given by $W_1 = \bar{s}e^{i\varphi}$, $W_2 = \bar{s}^2 e^{i2\varphi}$, and $W_3 = \bar{s}^3 \bar{z}e^{i3\varphi}$. The corresponding normalization integrals read $I_1 = (1/2\lambda)B\left(2, \frac{3}{2}\right.$
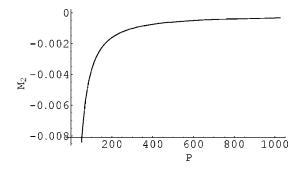

FIG. 2. The SHG dimensionless coupling matrix element $\bar{M}_2(P)$ as a function of P for $N_0 = 10^6$ in a spherical symmetry trap. Two $n_r l$ modes are 01 and 10.
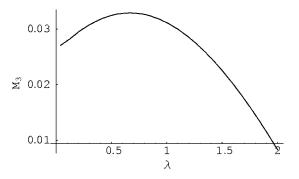
FIG. 3. The TWRI dimensionless coupling matrix element $\bar{M}_3(\lambda)$ as a function of the trap anisotropy λ for $P = 100$ and $N_0 = 10^6$ with a axially symmetric trap. The three $n_z n_s m$ modes are 001, 002, and 103.

$+q)B\left(\frac{1}{2}, 1+q\right)$, $I_2 = (1/2\lambda)B\left(3, \frac{3}{2}+q\right)B\left(\frac{1}{2}, 1+q\right)$, and $I_3 = (1/2\lambda^3)B\left(4, \frac{5}{2}+q\right)B\left(\frac{3}{2}, 1+q\right)$. The explicit expression for the dimensionless coupling matrix element then becomes

$$\bar{M}_3 = \frac{[4P/B(3/2, 2+q)]^{1/10}}{8\pi \lambda^{19/10} \sqrt{I_1 I_2 I_3 \bar{\omega}_1 \bar{\omega}_2 \bar{\omega}_3}} \sqrt{\frac{N_0}{P}}$$
$$\times \left[3\frac{\zeta^2}{q} \bar{\omega}_1 \bar{\omega}_2 \bar{\omega}_3 B(4, 1+2q) - \frac{\bar{\Delta}_3}{1+q} B(4, 3+2q) \right]. \tag{37}$$

The theoretical curve $\bar{M}_3(\lambda)$ is plotted in Fig. 3. It is important to note that $\bar{M}_3$ is dominated by the mismatching term (i.e., the term proportional to $\bar{\Delta}_3$) and affected a little by the contribution from ζ^2 term.

We then choose three $n_z n_s m$ modes 001, 010, and 101 in the TMRI. Their excitation spectra in the leading-order approximation are given by $\bar{\omega}_1^{(0)} = \sqrt{1+q}$, $\bar{\omega}_2^{(0)} = \{2 + \frac{3}{2}\lambda^2 + q - [4 - 4\lambda^2 + \frac{9}{4}\lambda^4 + (4 - 3\lambda^2 + q)q]^{1/2}\}^{1/2}$, and $\bar{\omega}_3^{(0)} = \sqrt{(1+\lambda^2)(1+q)}$. The functions are $W_1 = \bar{s}e^{i\varphi}$, $W_2 = 1 + b\bar{z}^2 + c\bar{s}^2$, and $W_3 = \bar{s}\bar{z}e^{i\varphi}$. The corresponding normalization integrals read

$$I_1 = (1/2\lambda)B\left(2, \frac{3}{2}+q\right)B\left(\frac{1}{2}, 1+q\right),$$

$$I_2 = (1/2\lambda)\left[1/(3/2+q) + 2cB\left(2, \frac{3}{2}+q\right)\right.$$
$$\left. + c^2 B\left(3, \frac{3}{2}+q\right)\right]B\left(\frac{1}{2}, 1+q\right) + (2b/\lambda^2)\left[1/(5/2+q)\right.$$
$$\left. + cB\left(2, \frac{5}{2}+q\right)\right]B\left(\frac{3}{2}, 1+q\right) + (b^2/\lambda^4)$$
$$\times[B(5/2, 1+q)/(7/2+q)],$$

and $I_3 = (1/2\lambda^3)B\left(2, \frac{5}{2}+q\right)B\left(\frac{3}{2}, 1+q\right)$. In mode 2, the condensate oscillates along the z axis, and the axial and radial oscillations have relative amplitude $b/c = \bar{\omega}_2^2 - 4 - 2q$ with $c \equiv \bar{\omega}_2^2/(2+2q-\bar{\omega}_2^2)$. Note that at $\bar{\omega}_2 = \sqrt{2+2q}$ the axial and radial amplitudes are divergent. Figure 4 shows such divergence behavior at $\lambda_c = 1.303$ by plotting c against the trap anisotropy λ with $P = 100$. In the $\lambda < \lambda_c$ region c is positive, while in the $\lambda > \lambda_c$ region c is negative. I_2 displays a very sharp peak at $\lambda = \lambda_c$. Figure 5 shows the $\bar{M}_3(\lambda)$ curve for this three-mode coupling. At $\lambda < (>) \lambda_c$ the positive (negative)
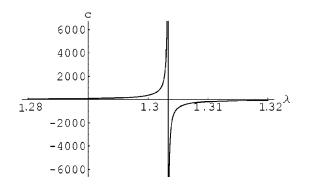
FIG. 4. The radial amplitude c (including the axial amplitude $b \propto c$) against the trap anisotropy λ for the 101 quadrupole mode. A divergence appears at $\lambda_c = 1.303$.

$\bar{M}_3$ increases slightly on increasing λ due to the jump of $\bar{M}_3 \propto c/\sqrt{I_2}$ at $\lambda = \lambda_c$ where the strongest resonance arises. It was shown that the $\bar{\Delta}_3$ term dominates the coupling process.

We finally calculate the coupling matrix element for a SHG. We choose two $n_z n_s m$ modes 010 and 200. The excitation spectra are $\bar{\omega}_{1,2}^{(0)} = \{2 + \frac{3}{2}\lambda^2 + q \mp [4 - 4\lambda^2 + \frac{9}{4}\lambda^4 + (4 - 3\lambda^2 + q)q]^{1/2}\}^{1/2}$ and the functions are given by $W_n = 1 + b_n \bar{z}^2 + c_n \bar{s}^2$ with the corresponding axial and radial amplitudes b_n and c_n ($n = 1, 2$). Figure 6 shows the $\bar{M}_2(\lambda)$ curve for this two-mode coupling. It was shown that the $\bar{\Delta}_2$ term dominates the coupling process. The integrand contained in W_1^2 as a function of the trap anisotropy λ has a peak at λ_c. The combination of the peaks contained in W_1^2 and the zero points contained in $1/I_1$ make $\bar{M}_2$ a continuous function of λ with two maxima at $\lambda = \lambda_c^\mp$. The strongest resonances occur at $\lambda_c^\mp$, determined by $2\bar{\omega}_1 = \bar{\omega}_2$, which has roots of $\lambda_c^\mp = \frac{1}{6}\{77 + 51q \mp 5[145 + 3(74 + 27q)q]^{1/2}\}^{1/2}$ in the leading order of $\bar{\omega}_{1,2}^{(0)}$. By taking $P = 100$ and $N_0 = 10^6$ we get $\lambda_c^- = 0.924$ for $q = 0.7$, and $\lambda_c^+ = 2.022$ for $q = 0.1$. As a special case, in the TF limit ($q = 0$) one has $\lambda_c^- = 0.683$ and $\lambda_c^+ = 1.952$, which have been obtained already in Refs. [2,13].

IV. NONLINEAR AMPLITUDES FOR TMRI AND SHG

A. Solutions of the TMRI and SHG envelope equations

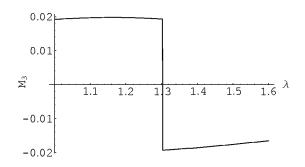With the dissipation-free coupling matrix elements in hand we now turn to look for the nonlinear amplitudes b_j for

FIG. 5. Same as Fig. 3 for the three 001, 010, and 101 modes. The strongest resonant coupling occurs at $\lambda_c = 1.303$.
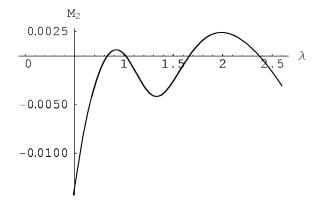

FIG. 6. The dimensionless SHG coupling matrix element $\bar{M}_2(\lambda)$ as a function of the trap anisotropy λ for $P = 100$, $N_0 = 10^6$, and fixed $q = 0.7$ with an axially symmetric trap. The two $n_z n_s m$ modes are 100 and 010. The maximal resonant coupling is located at $\lambda_c^- = 0.924$ and $\lambda_c^+ = 2.022$.

the TWRI and SHG processes. Note that the solutions of Eqs. (14)–(16), (22), and (23) have been studied in nonlinear optics [28] with the forms of $b_n(t) = |b_n(t)|\exp[i\varphi_n(t)]$ for $n = 1, 2, 3$. The general solutions can be expressed by the elliptic integrals $sn[x, y]$. For the SHG with initial amplitude $b_{10} = b_1(0)$ the solutions of Eqs. (22) and (23) read

$$b_2(t) = \frac{1}{\sqrt{2}} A_- b_{10} \text{sn}[t/t_2, A_-/A_+] \exp\left[-i\left(2\varphi_{10} + \frac{\pi}{2} + \frac{1}{2}\Delta_2 t\right)\right],$$

(38)

$$b_1(t) = \pm \sqrt{b_{10}^2 - 2|b_2(t)|^2} \exp\left[-i\left(\varphi_{10} + \frac{\pi}{4} + \frac{3}{4}\Delta_2 t - \frac{1}{2}\cos^{-1}\frac{\bar{\Delta}_2|b_2(t)|}{4\pi P\bar{M}_2|b_1(t)|^2}\right)\right],$$

(39)

where $A_\pm^2 = 1 + \frac{1}{2}\epsilon_2 \pm \sqrt{\epsilon_2(1 + \epsilon_2/4)}$ (i.e., the amplitudes are on the order of 1), $\epsilon_k = (\sqrt{2}\bar{\Delta}_k/8\pi P\bar{M}_k)^2$ are the relative frequency mismatches for $k = 2$ (3) in the SHG (TMRI) process, $t_k = |2\sqrt{2}\pi A_+ b_{10} P\bar{M}_k \omega_\perp|^{-1}$ are the time scales, and we note that $t_2 \simeq 10$ ms for most experiments. We see that the amplitudes change periodically for $\epsilon_2 \neq 0$, with a period $T_k \equiv F(1/2, 1/2, 1, A_-^2/A_+^2)/|\sqrt{2}\pi A_+ b_{10} P\bar{M}_k \omega_\perp|$ ($k = 2, 3$). In the case on resonance ($\bar{\Delta}_2 = 0$), the solutions become monotonic with respect to time t: $b_1(t) = \pm b_{10} \text{sech}(t/t_2)\exp(-i\varphi_{10})$ and $b_2(t) = (b_{10}/\sqrt{2})\tanh(t/t_2)\exp[-i(2\varphi_{10} + \pi/2)]$. Note that the phase difference between b_2 and b_1 is $\varphi_{10} + \pi/2$.

For the TMRI with initial amplitudes b_{10} and b_{20} the solutions Eqs. (14)–(16) are

$$b_3(t) = \frac{1}{\sqrt{2}} A_- b_{10} \text{sn}[t/t_3, A_-/A_+]$$

$$\times \exp\left[-i\left(\varphi_{10} + \varphi_{20} + \frac{\pi}{2} + \frac{1}{2}\Delta_3 t\right)\right],$$

(40)

$$b_n(t) = \pm \sqrt{b_{n0}^2 - 2|b_3(t)|^2} \exp[-i\varphi_n(t)] \quad (n=1,2),$$

$$(41)$$

where $A_{\pm}^2 = \frac{1}{2}[1+\sigma+\epsilon_3 \pm \sqrt{(1+\sigma+\epsilon_3)^2-4\sigma}]$, $\sigma = |b_{20}/b_{10}|^2$, $\varphi_n(t) = \Delta_3 \int_0^t dt |b_3(t)|^2/|b_n(t)|^2$ $(n=1,2)$, and $t_3 \simeq 5$ ms. We see that the initial value of mode 3 is zero and it increases from zero as time increases (it is generally a periodic function of time). In the case on resonance, i.e., $\bar{\Delta}_3 = 0$, the expressions for $A_{\pm}$ are simplified to $A_{+(-)} = 1$ (b_{20}/b_{10}) for $|b_{20}| < |b_{10}|$ and $A_{+(-)} = b_{10}/b_{20}$ (1) for $|b_{10}| < |b_{20}|$. The corresponding solutions $b_3(t) = (A_- b_{10}/\sqrt{2})\text{sn}[t/t_3, A_-/A_+]\exp[-i(\varphi_{10}+\varphi_{20}+\pi/2)]$ and $b_n(t) = \pm\sqrt{b_{n0}^2 - 2|b_3(t)|^2}\exp(-i\varphi_{n0})$ $(n=1,2)$ are still periodic in time with a period T_3.

B. Oscillations of the average squared widths of the condensate

We now discuss the oscillating behavior of the average squared widths (ASWs) of the condensate in the processes of TMRI and SHG, which are important physical quantities relevant to the experimental measurements [12]. Based on the results given in Ref. [20] we obtain the solutions for the field operator $\psi(\mathbf{r},t)$ at zero temperature,

$$\psi(\mathbf{r},t) = \lambda\sqrt{N_0}[2\pi R_\perp^3 B(3/2, 2+q)]^{-1/2}(1-\bar{r}^2)^{(q+1)/2}\Theta(1-\bar{r})$$

$$+ \sum_{n=1}^{k}[u_n(\mathbf{r})b_n(t)\exp(-i\omega_n t) + v_n^*(\mathbf{r})b_n^*(t)\exp(i\omega_n t)]$$

$$(42)$$

for the SHG $(k=2)$ and TMRI $(k=3)$ processes. The ASWs in the radial and axial directions are given by [29]

$$\langle \bar{\mathbf{r}}^2 \rangle = N_0^{-1}\langle \psi_G(\mathbf{r})|\bar{\mathbf{r}}^2|\psi_G(\mathbf{r})\rangle + N_0^{-1/2}\langle\psi_G(\mathbf{r})|\bar{\mathbf{r}}^2|\phi^{(1)}(\mathbf{r},t)\rangle$$

$$+\langle\phi^{(1)}(\mathbf{r},t)|\bar{\mathbf{r}}^2|\phi^{(1)}(\mathbf{r},t)\rangle. \quad (43)$$

The first term of Eq. (43) $(\bar{r}_G^2)$ comes from the ground-state background, the middle term $(\bar{r}_1^2)$ is a first-order oscillation (proportional to $|b_n|$ with the fundamental-mode frequency ω_n), and the last term $(\bar{r}_2^2)$ is a second-order oscillation (proportional to $|b_n|^2$ due to the mixing of sum- and difference-frequency modes with the frequency $\omega_n \pm \omega_{n'}$).

For $\lambda = 1$ (i.e., spheral trap), the radial ASWs are $\bar{r}_G^2 = 3/7$ for $q=0$,

$$\bar{r}_1^2 = \frac{3\zeta}{\sqrt{2\pi B[3/2, 2+q]}}\sum_{n=1}^{k}\frac{\delta_{l0}\bar{\omega}_{n_r l}^{(0)}}{n_r^2-1/4}\sqrt{\frac{2}{I_{n_r l}}}|b_n(t)|\cos(\varphi_n+\omega_n t)$$

(nonzero values with $l=0$), and

$$\bar{r}_2^2 = \int_0^1 \bar{r}^2 d\bar{r}\sum_{n=1}^{k}\left\{|b_n(t)|^2[|u_n|^2+|v_n|^2+2|u_n||v_n|\cos 2(\varphi_n\right.$$

$$\left.+\omega_n t)] + \sum_{n'\neq n}^{k}[u_n v_{n'}b_n b_{n'}\exp i(\omega_n+\omega_{n'})+\text{c.c.}]\right\}.$$

For $\lambda \notin 1$ (i.e., axial trap), the radial and axial ASWs are given by $\bar{s}_G^2 = 2/7$ and $\bar{z}_G^2 = \lambda^{-2}/7$ for $q=0$, $\bar{s}_1^2 \propto \bar{z}_1^2 \propto \delta_{m0}|b_n(t)|$
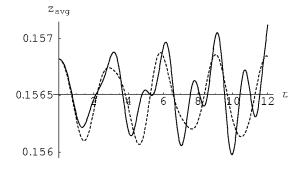

FIG. 7. The average axial width in units of $R_\perp$ vs t in units of $\omega_\perp^{-1}$ in the SHG process from the lower 010 mode to the higher 200 mode for $|b_{10}|=0.05$, $\varphi_0=0$, $P=100$, $N_0=10^6$, and fixed $q=0.7$ with an axially symmetric trap. The solid line is for the matched (on-resonance) case ($\lambda=2.415$), which shows clearly generation of the second-harmonic mode 200. The dashed line is for the mismatched (off-resonance) case ($\lambda=2.000$).

(nonzero values with $m=0$ for the first-order small vibrations), and $\bar{s}_2^2 \propto \bar{z}_2^2 \propto |b_n(t)|^2$ for the second-order small vibrations. Note that $\int_0^1 \bar{r}^2 d\bar{r}(|u_n|^2+|v_n|^2) = \frac{1}{2}\int_0^1 \bar{r}^2 d\bar{r}(\varphi_+^2+\varphi_-^2) \propto \zeta\Gamma(q)+\text{const}/\zeta$ for $q\to 0$; the ASWs are divergent in the TF limit (i.e., $P\to\infty$). Here divergence-free results are obtained by going beyond the TF limit (i.e., the TF regime $P \gg 1$).

The evolutions of the axial and radial ASWs of the BEC in the axially symmetric trap are shown, respectively, in Figs. 7 and 8 for the SHG process from the lower 010 mode to higher 200 mode with $|b_{10}|=0.05$ and $\varphi_{10}=0$ for the parameters $P=100$ and $N_0=10^6$. A resonant nonlinear coupling between the fundamental mode 010 and the second-harmonic mode 200 happens under the phase-matching condition $2\omega_1 = \omega_2$, which requires $\lambda=\lambda_c=2.415$ for $q=0.7$. The dashed lines for the mismatched (off-resonance) case ($\lambda=2.000$) show an oscillation of the lower 010 mode. In this case the second-harmonic mode (i.e., the 200 mode) is not generated. The solid lines in the figures are for the matched (on-resonance) case ($\lambda=2.415$), and show clearly the generation of the second-harmonic mode. The generation of the 200
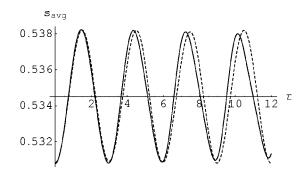

FIG. 8. The average radial width in units of $R_\perp$ vs t in units of $\omega_\perp^{-1}$ in the SHG process from the lower 010 mode to the higher 200 mode for $|b_{10}|=0.05$, $\varphi_0=0$, $P=100$, $N_0=10^6$, and fixed $q=0.7$ with an axially symmetric trap. The solid line is for the matched case ($\lambda=2.415$) and the dashed line is for the mismatched case ($\lambda=2.000$). There is no manifestation of the SHG from the radial ASWs.
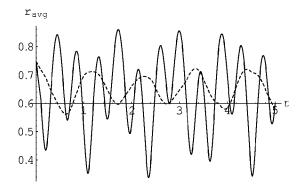
FIG. 9. The average radial width of the condensate in units of $R_\perp$ vs t in units of $\omega_\perp^{-1}$ in the TMRI process from the lower 20 and 30 modes to the higher 60 mode for $b_{10}=0.03$, $b_{20}=0.06$, $\varphi_{10}=\varphi_{20}=0$, and $N_0=10^6$ under the phase-matching condition $P=49$ and for a spherical symmetry trap. The solid line shows the generation of the higher 60 mode while the dashed line shows the time evolution of the lower modes.

mode here is due to the strong resonance between the 010 mode and the 200 mode and hence the energy of the 101 mode transfers into the 200 mode in the most efficient way when the phase-matching condition is exactly satisfied. However, due to the symmetry of these modes, the second-harmonic generation is manifested only in the axial oscillation. Thus if one explores the SHG according to the measurement of the ASWs for a BEC in an axially symmetric trap with the above selected modes, it is useless to measure the radial ASW. One must measure the axial ASW which displays strong signals for the SHG. This result agrees well with the experiment done by Hechenblaikner *et al.* [12]. The reason our theoretical curves fit well the experimental ones [12] is the following. For the 010 mode the function W [see Eq. (26)] is $W_1=1+b_1\bar{z}^2+c_1\bar{s}^2$. Both the axial and radial amplitudes b_1 and c_1 are divergent when the on-resonance condition $\bar{\omega}_1^2=2+2q$ is satisfied. However, the ratio of $|b_1/c_1|=|\bar{\omega}_1^2-4-2q|=2$, i.e., the oscillation amplitude in the z axis is greater than that in the xy plane. Therefore, the condensate oscillates along the axial direction and the SHG can be observed by measuring the axial ASW [12].

We now turn to discuss the three-mode resonant processes by using other different modes, which are not explored experimentally. The time evolution of the radial ASWs is
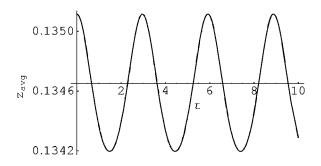

FIG. 10. The average radial width for a spherical trap in units of $R_\perp$ vs t in units of $\omega_\perp^{-1}$ in the SHG process from the lower 01 mode to the higher 10 mode for $b_{10}=0.05$, $\varphi_{10}=0$, and $N_0=10^6$ under the matching condition of $P=82$.

FIG. 11. The average axial width in units of $R_\perp$ vs t in units of $\omega_\perp^{-1}$ in the TWRI process from the lower 001 and 002 modes to the higher 103 mode for $|b_{10}|=0.03$, $|b_{20}|=0.06$, $\varphi_{10}=\varphi_{20}=0$, $P=100$, and $N_0=10^6$ with an axial symmetry trap of $\lambda_c=1.682$.

shown in Fig. 9 for a TMRI process in a BEC with a spherically symmetric trap with $b_{10}=0.03$, $b_{20}=0.06$, $\varphi_{10}=\varphi_{20}=0$, and $N_0=10^6$. The energy of the lower 20 and 30 modes transfers into the higher 60 mode under the matching condition $P=49$. Since $l_1=l_2=l_3=0$, there is a first-order vibration of the condensate with the oscillating frequencies $\omega_{1,2,3}$. The solid line denotes the vibrations of the radial ASW of the condensate, showing clearly the generation of the higher 60 mode. For comparison a dashed line is plotted to show the vibrations of the lower 20 and 30 modes.

Shown in Fig. 10 is the time evolution of the radial ASW of the condensate for the SHG process from the lower 01 mode to the higher 10 mode with $|b_{10}|=0.05$, $\varphi_{10}=0$, and $N_0=10^6$ under the matching condition of $P=82$ for a spherical trap. Because in this case we have $l_1=1$ and $l_2=0$, in the leading order there is no contribution to the oscillation of the ASW coming from the fundamental mode 01. The ASW oscillation is due to the contribution from the second-harmonic mode 10 (in the leading order) and the fundamental mode (in the second order).

Shown in Figs. 11 and 12 are, respectively, the time evolution of the axial and radial ASWs of an axially symmetric BEC in the TMRI process from the lower 001 and 002 modes to the higher 103 mode with $b_{10}=0.03$, $b_{20}=0.06$, and $\varphi_{10}=\varphi_{20}=0$ for the parameters $P=100$ and $N_0=10^6$ where the phase-matching condition is $\lambda_c=1.682$. Since in this case $\bar{s}_1^2=\bar{z}_1^2=0$ and $\bar{s}_2^2\propto\bar{z}_2^2=\int\bar{z}^2 d^3\bar{\mathbf{r}}\Sigma_{n=1}^k|b_n(t)|^2(|u_n|^2+|v_n|^2)$, there are only zero-frequency second-order oscillation coming

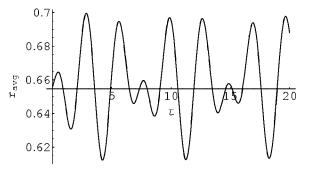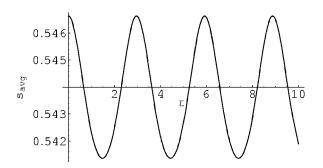FIG. 12. The average radial width in units of R_z vs t in units of $\omega_\perp^{-1}$ in the TWRI process from the lower 001 and 002 modes to the higher 103 mode for $|b_{10}|=0.03$, $|b_{20}|=0.06$, $\varphi_{10}=\varphi_{20}=0$, $P=100$, and $N_0=10^6$ with an axial symmetry trap of $\lambda_c=1.682$.

from the elliptic integrals. So there is energy transfer of up- and down-conversion within each time period $t=T_3$. In the time interval $0<t<T_3$, the system is in the lower 001 and 002 modes (i.e., $b_3\simeq0$). For $t>T_3$ the energy is transferred to the higher 103 mode (i.e., $b_{1,2}\simeq0$). The up-conversion occurs at $t=T_3$. However, there are no fundamental-mode frequency components appearing in the shape vibrations.

V. DISCUSSION AND SUMMARY

We have made a systematic investigation of the resonant mode coupling of the collective excitations in a harmonically trapped BEC at zero temperature with a repulsive inter-atomic interaction. We have proposed a divergence-free, con-sistent theory for describing low-energy collective excita-tions and their interactions in both the linear and nonlinear regimes beyond the TF limit. The nonlinearly coupled enve-lope equations for three-mode resonant interactions have been derived by use of the method of multiple scales. We have demonstrated how to calculate analytically the coupling matrix elements for mode-coupling problems in trapped BECs and how to eliminate the divergence appearing in the integrals of the coupling matrix elements by using a Fetter-like variational approximation for the ground-state wave function of the condensate. We have obtained the selection rules for mode-mode interaction processes according to the symmetry of the excitation modes. The divergence-free for-mulas for the average squared widths in the radial and axial directions have been given explicitly; they describe the shape oscillations of the condensate and can be compared with ex-perimental measurements directly. We have also shown that the calculations of the coupling matrix elements and shape oscillations can be simplified greatly by using the orthogo-nality relations of the eigenfunctions $u_n(\mathbf{r})$ and $v_n(\mathbf{r})$.

We have discussed in detail a set of three-mode resonant coupling processes (including SHG as a particular case) for spherically and axially symmetric traps. By solving the non-linearly coupled envelope equations we have obtained the nonlinear amplitudes and then made a detailed calculation of the shape oscillations of the condensate for different mode-coupling processes in different parameter regimes. The the-oretical results about the shape vibrations of the BEC for SHG in the case of an axially symmetric trap agree well with the experimental observations. We have also made theoreti-cal predictions on a series of TMRI processes, which need to be verified experimentally further. For example, for a BEC in a spherically symmetric trap, the first-order radial vibration of the condensate shape with the frequencies ω_{20}, ω_{30}, and ω_{60} may be measured by selecting the lower modes $n_r=2$, $l_1=0$ and $n_r=3$, $l_2=0$ (dashed line predicted in Fig. 9) and higher mode $n_r=6$, $l_3=0$ (solid line predicted in Fig. 9) with suitable parameters N_0 and $a_{\text{sc}}/a_{\text{HO}}$. We stress that although the theoretical description developed in this work is mainly for TMRI and SHG, a generalization to other mode-coupling processes is straightforward.

ACKNOWLEDGMENTS

[1] A. Fetter and J. D. Walecka, *Quantum Theory of Many-Particle Systems* (Dover, New York, 2003).

[2] F. Dalfovo *et al.*, Rev. Mod. Phys. **71**, 463 (1999); A. J. Leg-gett, *ibid.* **73**, 307 (2001).

[3] C. J. Pethick and H. Smith, *Bose-Einstein Condensation in Dilute Gases* (Cambridge University Press, Cambridge, U.K., 2003); L. Pitaevskii and S. Stringari, *Bose-Einstein Condensa-tion* (Clarendon, Oxford, 2003), and references therein.

[4] M. H. Anderson *et al.*, Science **269**, 198 (1995); K. B. Davis *et al.*, Phys. Rev. Lett. **75**, 3969 (1995); C. C. Bradley, C. A. Sackett, J. J. Tollett, and R. G. Hulet, *ibid.* **75**, 1687 (1995).

[5] S. Burger *et al.*, Phys. Rev. Lett. **83**, 5198 (1999); J. Den-schlag *et al.*, Science **287**, 97 (2000); Z. Dutton *et al.*, *ibid.* **293**, 663 (2001); K. E. Strecker *et al.*, Nature (London) **417**, 150 (2002); L. Khaykovich *et al.*, Science **296**, 1290 (2002).

[6] G. Huang, Manuel G. Velarde, and Valeri A. Makarov, Phys. Rev. A **64**, 013617 (2001); Guoxiang Huang, Jacob Szeftel, and Shanhua Zhu, *ibid.* **65**, 053605 (2002); Guoxiang Huang, V. A. Makarov, and M. G. Velarde, *ibid.* **67**, 023604 (2003).

[7] M. R. Matthews *et al.*, Phys. Rev. Lett. **83**, 2498 (1999); K. W. Madison, F. Chevy, W. Wohlleben, and J. Dalibard, *ibid.* **84**, 806 (2000); J. R. Abo-Shaeer *et al.*, Science **292**, 476 (2001).

[8] A. L. Fetter, Phys. Rev. A **53**, 4245 (1996).

[9] P. A. Ruprecht, Mark Edwards, K. Burnett, and Charles W. Clark, Phys. Rev. A **54**, 4178 (1996).

[10] F. Dalfovo, C. Minniti, and L. P. Pitaevskii, Phys. Rev. A **56**, 4855 (1997).

[11] S. Morgan, S. Choi, K. Burnett, and M. Edwards, Phys. Rev. A **57**, 3818 (1998).

[12] G. Hechenblaikner *et al.*, Phys. Rev. Lett. **85**, 692 (2000); E. Hodby, O. M. Maragò, G. Hechenblaikner, and C. J. Foot, Phys. Rev. Lett. **86**, 2196 (2001).

[13] G. Hechenblaikner, S. A. Morgan, E. Hodby, O. M. Maragò, and C. J. Foot, Phys. Rev. A **65**, 033612 (2002).

[14] R. Ozeri, N. Katz, J. Steinhauer, E. Rowen, and N. Davidson, Phys. Rev. Lett. **90**, 170401 (2003).

[15] O. M. Maragò *et al.*, Phys. Rev. Lett. **84**, 2056 (2000); U. Al Khawaja and H. T. C. Stoof, Phys. Rev. A **65**, 013605 (2001).

[16] L. Deng *et al.*, Nature (London) **398**, 218 (1999); M. Trippen-bach, Y. B. Band, and P. S. Julienne, Phys. Rev. A **62**, 023608 (2000).

[17] G. Huang, X.-q. Li, and J. Szeftel, Phys. Rev. A **69**, 065601 (2004); C. Sun, C. Hang, G. Huang, and B. Hu, Mod. Phys. Lett. B **18**, 375 (2004).

[18] P. Öhberg *et al.*, Phys. Rev. A **56**, R3346 (1997).

[19] M. Edwards, P. A. Ruprecht, K. Burnett, R. J. Dodd, and Charles W. Clark, Phys. Rev. Lett. **77**, 1671 (1996); Mark Edwards, R. J. Dodd, C. W. Clark, P. A. Ruprecht, and K.

Burnett, Phys. Rev. A **53**, R1950 (1996).

[20] B. Hu, G. Huang, and Y. L. Ma, Phys. Rev. A **69**, 063608 (2004). There is a misprint: $(7/2+q)$ should be replaced by $(7/2+q)^2$ in the second term on the right hand side of Eq. (13).

[21] A similar approach for finite temperature can be easily developed based on Bogoliubov quasiparticle approach, which will be given elsewhere.

[22] A. Jeffry and T. Kawahawa, *Asymptotic Methods in Nonlinear Wave Theory* (Pitman, London, 1982).

[23] One can generally include the contribution of the dc component (i.e., the zero mode) to Eq. (8) and hence some additional linear terms with coefficients proportional to the dc component appear on the right hand side of the nonlinearly coupled envelope Eqs. (14)–(16), (22), and (23). However, the contribution from these additional terms gives only a phase modification for the relevant mode b_j ($j \neq 0$). In the three-wave processes we are interested in here such terms are dependent on the initial incident condition and can be disregarded because in the experiment [12] no dc component is applied in the system.

[24] A slowly varying rectification field can be generated in the system by the interaction of excitations. However, the production of such rectification fields belongs to third- or higher-order nonlinear processes and are thus not relevant to our discussion (second-order processes) here.

[25] The definitions for the quantities $\bar{r}$, $\bar{s}$, etc., can be found in Ref. [20].

[26] Y. L. Ma and S. T. Chui, Phys. Rev. A **65**, 053610 (2002).

[27] D. McPeake and J. F. McCann, Phys. Rev. A **68**, 053610 (2003).

[28] J. A. Armstrong *et al.*, Phys. Rev. **127**, 1918 (1962).

[29] Y. L. Ma and S. T. Chui, J. Phys.: Condens. Matter **14**, 10105 (2002).